

Tuning selective reflection of light by surface anchoring in cholesteric cells with oblique helicoidal structures

OLENA S. IADLOVSKA¹², GRAHAM R. MAXWELL¹, GRETA BABAKHANOVA¹³, GEORG H. MEHL⁴, CHRISTOPHER WELCH⁴, SERGIJ V. SHIYANOVSKII¹³, AND OLEG D. LAVRENTOVICH^{123,*}

Affiliations:

¹*Liquid Crystal Institute, Kent State University, Kent, Ohio 44242, USA*

²*Department of Physics, Kent State University, Kent, Ohio 44242, USA*

³*Chemical Physics Interdisciplinary Program, Kent State University, Kent, Ohio 44242, USA*

⁴*Department of Chemistry, University of Hull, Hull HU6 7RX, UK*

*olavrent@kent.edu

ABSTRACT

Selective reflection of light by oblique helicoidal cholesteric (Ch_{OH}) can be tuned in a very broad spectral range by an applied electric field. In this work, we demonstrate that the peak wavelength of the selective reflection can be controlled by surface alignment of the director in sandwich cells. The peak wavelength is blue-shifted when the surface alignment is perpendicular to the bounding plates and red-shifted when it is planar. The effect is explained by the electric field redistribution within the cell caused by spatially varying helicoidal Ch_{OH} structure. The observed phenomenon can be used in sensing applications.

INTRODUCTION

Cholesteric liquid crystals (Ch) with periodically twisted arrangements of molecules are known as the prime example of the material with the so-called structural color [1, 2]. Since the period of the structure is often in the range of few hundreds of nanometers, Ch is capable of selective reflection of light in the visible part of spectrum. Recently it has been demonstrated that the peak wavelength and the band width of light reflection can be controlled by an electric [3-5] or a magnetic field [6]. The tunability is achieved when the

material exhibits a small bend elastic constant [3, 7, 8]. Upon application of the field, such a material forms an oblique helicoidal structure, abbreviated as Ch_{OH} , in which the local director twists around the direction of the field and makes an acute angle θ with this direction. A non-zero projection of the director onto the field direction ensures a finite aligning field torque which controls the period of the structure. In a regular Ch, the molecules are perpendicular to the helicoidal axis and such a tunability is impossible.

Here we demonstrate that the peak wavelength and the bandwidth of selective reflection of light at the oblique helicoidal Ch_{OH} can be controlled by surface alignment: the wavelength of Bragg reflection is blue-shifted when the alignment is perpendicular (homeotropic) and red-shifted when it is planar.

RESULTS AND DISCUSSION

Materials and measurement techniques. We prepared a Ch_{OH} mixture with a small bend constant K_3 at temperatures close to the room temperature. The components of the mixture are dimeric compounds 1'',7'' - bis(4-cyanobiphenyl-4'-yl) heptane (CB7CB) and 1'',11''- bis(4-cyanobiphenyl-4'-yl) undecane (CB11CB), rod-like mesogen pentylcyanobiphenyl (5CB) (Merck), and left-handed chiral dopant S811 (Merck), in weight proportion 5CB:CB7CB:CB11CB:S811 = 49.8:30:16:4.2. At $T_{\text{Ch-I}} = 60.7^\circ\text{C}$, the Ch phase melts into an isotropic fluid, and at $T_{\text{Ch-Ch}_b} = 24.5^\circ\text{C}$ it transforms into the chiral analog of the twist-bend nematic [9-11]. The experiments were performed at $T = 27.5^\circ\text{C}$. The temperature was controlled by a hot stage HCS402 with temperature controller mK2000 (both Instec, Inc.) with the accuracy 0.01°C .

Planar cells were assembled from glass plates with transparent indium tin oxide (ITO) electrodes and a layer of rubbed polyimide PI2555. Homeotropic cells were assembled from ITO-coated glass plates spin-coated with a polyimide SE5661 (Nissan Chemical Industries) and then additionally coated with 1% water solution of Dimethyloctadecyl[3-(trimethoxysilyl)propyl] ammonium chloride (Sigma-Aldrich) [12]. The cell thicknesses were set by spherical spacers mixed with UV-curable glue NOA 68 (Norland Products, Inc.). The cell thickness was measured by the light interference technique. We report data for a planar cell with $d = 23.7 \mu\text{m}$ and for a homeotropic cell with $d = 23.5 \mu\text{m}$.

An AC voltage of frequency 3 kHz (sinusoidal mode, DS345 waveform generator (Stanford Research) and 7602-M voltage amplifier (KROHN-HITE Co.)) is applied to the ITO electrodes. Since the mixture is of a positive dielectric anisotropy, the electric field causes formation of the heliconical director structure with the axis $\hat{\mathbf{t}}$ perpendicular to the glass plates and parallel to the field, $\hat{\mathbf{t}} \parallel \mathbf{E}$. The heliconical structure is stable in the range $(0.6-1.1) \text{ V}/\mu\text{m}$, changing its period with the field. When the field changes, the peak

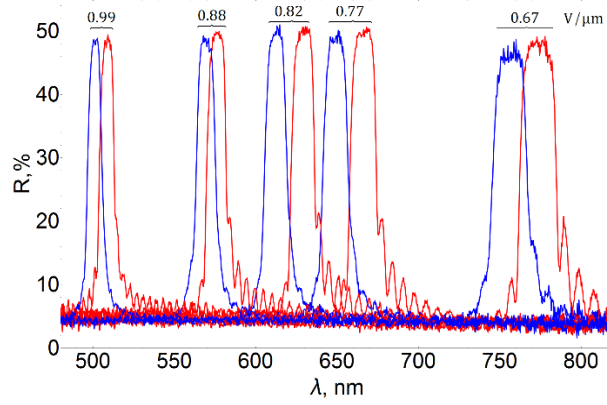


Fig. 1. (Color online.) Selective Bragg reflection in cells with homeotropic (blue) and planar (red) surface alignment under the applied electric field $E_{app} = U/d$. Values of E_{app} are indicated above the reflection peaks in V/ μ m.

wavelength λ_{max} of Bragg reflection moves from UV to near IR, as described in Refs. [3, 4]. The Bragg reflection is characterized by using USB2000 spectrometer and tungsten halogen light source LS-1 (both Ocean Optics). LS-1 generates a white unpolarized beam that is focused by the lens into a paraxial ray impinging normally onto the cells. λ_{max} was determined by finding the full width of the reflection peak at its half-amplitude $\Delta\lambda$ and then defining λ_{max} as the coordinate of the middle of the full width.

Optical spectra results and discussion. Figure 1 shows that the planar and homeotropic Ch_{OH} cells of practically identical thickness d , being subject to the same electric field $E_{app} = U/d$, where U is the voltage, produce different wavelength λ_{max} of Bragg reflection. The homeotropic cell shows a blue-shifted reflection, while the planar cell shows a red-shifted reflection. The separation of the two peaks varies from 32 – 35 nm in the 750-800 nm region to 6-7 nm in the 500-550 nm region, Fig.1.

The field dependences of λ_{max} for the homeotropic and planar cells are plotted in Fig. 2 (a). The difference is clear if the data are presented as $\lambda_{max} E_{app}$ vs. E_{app} , Fig. 2 (b). Although the planar cell shows wider peaks as compared to the homeotropic cell, this difference is small, Fig. 2 (c). The difference in spectral response is not related to the small difference in cell thicknesses, as the data in Figs. 1-2 are presented as functions of the field rather than the voltage.

To understand the mechanism behind the anchoring sensitivity of reflection, let us first recall the Ch_{OH} features. The Ch_{OH} appears under the action of electric field $\mathbf{E} = E\hat{\mathbf{z}}$ in order to minimize the free energy density [7, 13]:

$$f = \frac{1}{2} \left\{ K_1 (\nabla \cdot \hat{\mathbf{n}})^2 + K_2 [\hat{\mathbf{n}} \cdot (\nabla \times \hat{\mathbf{n}}) - q_0]^2 + K_3 [\hat{\mathbf{n}} \times (\nabla \times \hat{\mathbf{n}})]^2 - \mathbf{D} \cdot \mathbf{E} \right\}, \quad (1)$$

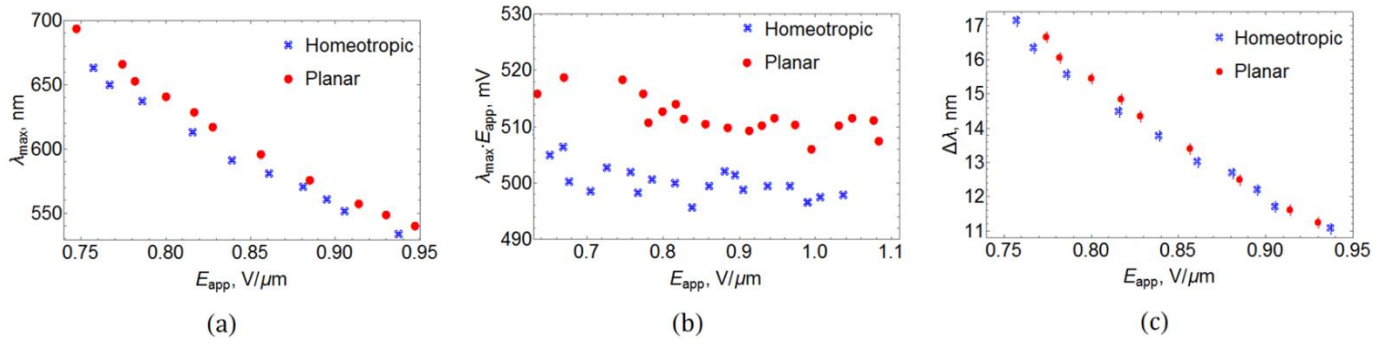


Fig.2. (Color online.) The wavelength λ_{\max} (a), product $\lambda_{\max} E_{app}$ (b), and bandwidth $\Delta\lambda$ (c) of reflection peaks in homeotropic (blue) and planar (red) cells as functions of applied electric field E_{app} .

where K_1 and K_2 are the elastic constants of splay and twist, respectively; $q_0 = 2\pi/P_0$ is the field-free value of the wave-vector; the pitch P_0 is determined by the chemical composition; $\mathbf{D} = \varepsilon_0 \varepsilon \mathbf{E}$ is the electric displacement, ε_0 is the dielectric constant and ε is the tensor of dielectric permittivity with the two principal components ε_{\parallel} and ε_{\perp} , parallel and perpendicular to the director, respectively. For an infinitely thick ChOH cell considered in Refs. [3, 7, 8], the equilibrium director writes in Cartesian coordinates (x, y, z) as

$$n_x = \cos \varphi \sin \theta_{\infty}; \quad n_y = -\sin \varphi \sin \theta_{\infty}; \quad n_z = \cos \theta_{\infty}, \quad (2)$$

where $\varphi = qz + \text{const}$ is the angle of the director's azimuthal orientation, $q = 2\pi/P$; the pitch P and the polar conical angle θ_{∞} between the local director and $\hat{\mathbf{t}}$ are both field-dependent:

$$P = \frac{2\pi}{E} \sqrt{\frac{K_3}{\varepsilon_0 \Delta\varepsilon}}, \quad (3)$$

$$\sin^2 \theta_{\infty} = \frac{\kappa}{1-\kappa} \left(\frac{E_{NC}}{E} - 1 \right). \quad (4)$$

Here, $\Delta\varepsilon = \varepsilon_{\parallel} - \varepsilon_{\perp}$, $\kappa = K_3/K_2$ and $E_{NC} = 2\pi K_2/P_0 \sqrt{\varepsilon_0 \Delta\varepsilon K_3}$ is the field at which the oblique helicoid unwinds into a uniform uniaxial nematic.

The peak wavelength of reflection at an infinitely thick ChOH cell is $\lambda_{\max}^{\infty} = \bar{n}_{eff} P$, where $\bar{n}_{eff} = (n_o + n_{e,eff})/2$ is the average refractive index, and $n_{e,eff} = n_o n_e / \sqrt{n_e^2 \cos^2 \theta_{\infty} + n_o^2 \sin^2 \theta_{\infty}}$ is the effective extraordinary index. With Eq. (3), the field dependency writes

$$\lambda_{\max}^{\infty} = \frac{2\pi \bar{n}_{eff}}{E} \sqrt{\frac{K_3}{\varepsilon_0 \Delta\varepsilon}}. \quad (5)$$

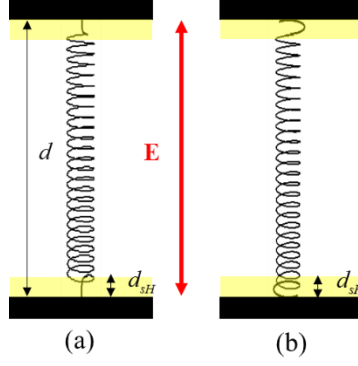


Fig.3. Schemes of ChOH cells with director deformation in surface regions for homeotropic (a) and planar (b) alignment.

The bandwidth of reflection is $\Delta\lambda = \Delta n_{\text{eff}} \cdot P$, where $\Delta n_{\text{eff}} = n_{e,\text{eff}} - n_o \approx (n_e^2 - n_o^2)n_o \sin^2 \theta_\infty / 2n_e^2$. Using Eqs. (3), (4) and the definition of E_{NC} above, one concludes that the bandwidth is also tunable by the field:

$$\Delta\lambda_\infty = \frac{\kappa^2 E_{NC} P_0 n_o}{2E(1-\kappa)} \left(1 - \frac{n_o^2}{n_e^2}\right) \left(\frac{E_{NC}}{E} - 1\right). \quad (6)$$

Figure 3 illustrates how the heliconal ChOH is influenced by the surface anchoring in cells. In the homeotropic cell, the conical angle $\theta(z)$ near the bounding plates depends on the vertical coordinate z and remains smaller than θ_{bulk} , Fig.3 (a). In the planar cell, the subsurface angle $\theta(z)$ is larger than θ_{bulk} , Fig. 3 (b). The structure in the center of cells is similar to the uniform oblique helicoid. The spatial variation $\theta(z)$ implies a variation of dielectric permittivity and thus, spatial variation of the local electric field. To describe the field distribution, we consider the cells as being comprised of three regions. In the homeotropic cell, there are two subsurface regions of a small thickness d_{sH} in which θ changes from 0 at the substrates to some value θ_{bulkH} , and a central region of thickness $d - 2d_{sH}$, where $\theta = \theta_{\text{bulkH}} = \text{const}$. In all three regions, the electric displacement along the z -axis, $D_z = \epsilon_0 \epsilon_{zz}(z) E_z(z) = \text{const}$, is independent of the z -coordinate; here $\epsilon_{zz}(z) = \epsilon_\perp \sin^2 \theta(z) + \epsilon_\parallel \cos^2 \theta(z)$ and $E_z(z)$ is the spatially varying electric field. The model allows us to present the applied voltage through D_z :

$$U = 2d_{sH} \frac{D_z}{\epsilon_0 \epsilon_{sH}} + (d - 2d_{sH}) \frac{D_z}{\epsilon_0 \epsilon_{\text{bulkH}}}, \quad (7)$$

where $\epsilon_{sH} = (\epsilon_{\text{bulkH}} + \epsilon_\parallel) / 2$ is the effective permittivity of the two subsurface regions, ϵ_{bulkH} is the permittivity of the central region with $\epsilon_{\text{bulkH}} = \epsilon_\perp \sin^2 \theta_{\text{bulkH}} + \epsilon_\parallel \cos^2 \theta_{\text{bulkH}}$.

The value of d_{sH} is much smaller than d and determined by the elastic response of the helicoid to the surface alignment. Since the heliconical structure in the surface regions is not well defined, the measured selective reflection of light is determined mostly by the reflection from the central part with $\theta_{bulkH} = \text{const}$. The peak wavelength of this reflection can be described similarly to Eq.(5) in which $E = E_{bulkH} = D_z / \varepsilon_0 \varepsilon_{bulk}$. The peak $\lambda_{\max H}$ of reflection at a homeotropic cell of finite thickness can be written as a product of λ_{\max}^∞ and two correcting factors,

$$\lambda_{\max H} = \lambda_{\max}^\infty \eta_H \xi_H, \quad \eta_H = \frac{\bar{n}_{bulkH}}{\bar{n}_{eff}}, \quad \xi_H = 1 - 2 \frac{d_{sH}}{d} \left(1 - \frac{\varepsilon_{bulkH}}{\varepsilon_{sH}} \right); \quad (8)$$

here $\bar{n}_{bulkH} = n_o / 2 + n_o n_e / 2 \sqrt{n_e^2 + (n_o^2 - n_e^2) \sin^2 \theta_{bulkH}}$. Both correcting factors are smaller than 1. In Eq. (8), $\varepsilon_{bulkH} < \varepsilon_{sH}$, where ε_{sH} is approaching ε_{\parallel} because of the surface alignment; therefore, $\xi_H < 1$. Furthermore, $\theta_{bulkH} < \theta_\infty$, thus $\bar{n}_{bulkH} < \bar{n}_{eff}$ and $\eta_H < 1$. We conclude that both ξ_H and η_H favor a blue-shifted reflection of light in a homeotropic cell as compared to an infinite slab of ChOH, i.e., $\lambda_{\max H} < \lambda_{\max}^\infty$.

The peak wavelength $\lambda_{\max P}$ of the planar cell is derived similarly, by introducing two surface regions d_{sP} , in which the cone angle varies from $\pi/2$ to $\theta_{bulkP} = \text{const}$, so that

$$\lambda_{\max P} = \lambda_{\max}^\infty \eta_P \xi_P, \quad \eta_P = \frac{\bar{n}_{bulkP}}{\bar{n}_{eff}}, \quad \xi_P = 1 - 2 \frac{d_{sP}}{d} \left(1 - \frac{\varepsilon_{bulkP}}{\varepsilon_{sP}} \right) \quad (9)$$

and $\varepsilon_{bulkP} = \varepsilon_{\perp} \sin^2 \theta_{bulkP} + \varepsilon_{\parallel} \cos^2 \theta_{bulkP}$, $\bar{n}_{bulkP} = n_o / 2 + n_o n_e / 2 \sqrt{n_e^2 + (n_o^2 - n_e^2) \sin^2 \theta_{bulkP}}$. Since $\theta_{bulkP} > \theta_\infty$ and $\varepsilon_{bulkP} > \varepsilon_{sP}$, one finds that $\eta_P > 1$ and $\xi_P > 1$, i.e. the reflection peak in a planar cell shifts towards the red end, $\lambda_{\max P} > \lambda_{\max}^\infty$, as observed.

In theory, the bandwidth $\Delta\lambda = \Delta n_{eff} \cdot P$ depends on P and on Δn_{eff} ; its experimental value is also influenced by nonuniformity of the textures. The difference in $\Delta\lambda$ between the homeotropic and planar cells is noticeable in the red part of spectrum, corresponding to the fields below 0.85 V/ μm , Fig. 2 (c). At higher fields, there is practically no difference. The effect can be caused by a relatively large separation of $\lambda_{\max H}$ and $\lambda_{\max P}$ in the red part of spectrum that yields a larger difference in the pitch. Nonuniformity of the textures is another factor making $\Delta\lambda$ for the two cells similar to each other.

The model explains the main experimental result, namely, blue and red shifts of Bragg reflection in homeotropic and planar cell. It has a clear physical meaning. In the homeotropic cell,

redistribution of the electric field is such that the bulk layer with a uniform Ch_{OH} is subject to an electric field that is higher than the average field U/d . In the planar cell, the effective field is weaker than U/d . Since the pitch is inversely proportional to the field, Eq.(3), the shift is blue in the homeotropic cell and red in the planar cell.

It is of interest to estimate d_s for the typical $\varepsilon_{\perp}, \varepsilon_{\parallel}, \varepsilon_{\text{bulk}}$. Assuming $d_{\text{SH}} \approx d_{\text{SP}}$, and $\varepsilon_{\text{bulkH}} \approx \varepsilon_{\text{bulkP}}$, one finds

$$\frac{d_s}{d} = c(\theta) \cdot \frac{\lambda_{\text{maxP}} - \lambda_{\text{maxH}}}{\lambda_{\text{maxH}}}, \quad (10)$$

where $c(\theta) = (\varepsilon_{\text{bulk}} + \varepsilon_{\parallel})(\varepsilon_{\text{bulk}} + \varepsilon_{\perp}) / 4(\varepsilon_{\parallel} - \varepsilon_{\perp})\varepsilon_{\text{bulk}}$ is a weak function of θ . With the permittivities measured in our laboratory, $\varepsilon_{\parallel} = 14.5$ and $\varepsilon_{\perp} = 6.4$, one finds $c(\theta) = 1.27 \pm 0.02$ when $0 < \theta < \pi/6$. Thus, d_s is about $0.4 \mu\text{m}$ in the region $500 - 600 \text{ nm}$ and $1 \mu\text{m}$ in the region $700-800 \text{ nm}$, i.e., much smaller than the cell thickness.

SUMMARY

We demonstrated a pronounced effect of confinement and alignment on Bragg reflection from the Ch_{OH} structure. The peak wavelength is red-shifted in planar Ch_{OH} cells and blue-shifted in homeotropic cells. The shifts are explained by redistribution of the electric field within the cell, caused by different director orientation in surface regions and nonlocal character of the dielectric coupling. The sensitivity of Bragg reflection to the surface alignment can be used as a tool to detect chemicals that are capable of changing the anchoring direction in liquid crystal cells, see, for example [14].

Funding. National Science Foundation grant DMR-1410378 and REU program CHE-1659571.

Acknowledgement. We thank Dr. T.J. White, Air Force Research Laboratory, Wright-Patterson Air Force Base, Ohio, for the supply of CB7CB.

REFERENCES

1. V. Sharma, M. Crne, J.O. Park, M. Srinivasarao, *Structural Origin of Circularly Polarized Iridescence in Jeweled Beetles*. Science, 2009. **325**(5939): p. 449-451.
2. Mitov, M., *Cholesteric liquid crystals in living matter*. Soft Matter, 2017. **13**(23): p. 4176-4209.

3. J. Xiang, S.V. Shiyonovskii, C.T. Imrie, and O.D. Lavrentovich, *Electrooptic Response of Chiral Nematic Liquid Crystals with Oblique Helicoidal Director*. Physical Review Letters, 2014. **112**(21): p. 217801.
4. J. Xiang, Ya. Li, Q. Li, D.A. Paterson, J.M.D. Storey, C.T. Imrie, and O.D. Lavrentovich, *Electrically Tunable Selective Reflection of Light from Ultraviolet to Visible and Infrared by Heliconical Cholesterics*. Advanced Materials, 2015. **27**(19): p. 3014-3018.
5. J. Xiang, A. Varanytsia, F. Minkowski, D.A. Paterson, J.M.D. Storey, C.T. Imrie, O.D. Lavrentovich and P. Palffy-Muhoray, *Electrically tunable laser based on oblique heliconical cholesteric liquid crystal*. Proceedings of the National Academy of Sciences of the United States of America, 2016. **113**(46): p. 12925-12928.
6. S.M. Salili, J. Xiang, H. Wang, Q. Li, D.A. Paterson, J.M.D. Storey, C.T. Imrie, O.D. Lavrentovich, S.N. Sprunt, J.T. Gleeson, A. Jákli, *Magnetically tunable selective reflection of light by heliconical cholesterics*. Physical Review E, 2016. **94**(4): p. 042705.
7. Meyer, R.B., *Effects of Electric and Magnetic Fields on the Structure of Cholesteric Liquid Crystals*. Applied Physics Letters, 1968. **12**(9): p. 281-282.
8. De Gennes, P.G., *Calcul de la distorsion d'une structure cholestérique par un champ magnétique*. Solid State Communications, 1968. **6**(3): p. 163-165.
9. M. Cestari, S. Diez-Berart, D. A. Dunmur, A. Ferrarini, M. R. de la Fuente, D. J. B. Jackson, D. O. Lopez, G. R. Luckhurst, M. A. Perez-Jubindo, R. M. Richardson, J. Salud, B. A. Timimi, and H. Zimmermann, *Phase behavior and properties of the liquid-crystal dimer 1'',7''-bis(4-cyanobiphenyl-4'-yl) heptane: a twist-bend nematic liquid crystal*. Phys Rev E 2011. **84**(3 Pt 1): p. 031704.
10. D. Chen, J.H. Porada, J.B. Hooper, A. Klittnick, Yo. Shen, M.R. Tuchband, E. Korblova, D.M. Walba, M.A. Glaser, J.E. MacLennan, and N.A. Clark, *Chiral heliconical ground state of nanoscale pitch in a nematic liquid crystal of achiral molecular dimers*. Proceedings of the National Academy of Sciences, 2013. **110**(40): p. 15931-15936.
11. V. Borshch, Y.-K. Kim, J. Xiang, M. Gao, A. Jákli, V.P. Panov, J.K. Vij, C.T. Imrie, M.G. Tamba, G.H. Mehl, and O.D. Lavrentovich, *Nematic twist-bend phase with nanoscale modulation of molecular orientation*. Nature Communications, 2013. **4**: p. 2635.
12. G. Cukrov, Yo. M. Golestani, J. Xiang, Yu.A. Nastishin, Z. Ahmed, C. Welch, G.H. Mehl, and O.D. Lavrentovich, *Comparative analysis of anisotropic material properties of uniaxial nematics formed by flexible dimers and rod-like monomers*. Liquid Crystals, 2017. **44**(1): p. 219-231.
13. de Gennes, P.G. and J. Prost, *The Physics of Liquid Crystals*. 1993, Oxford: Clarendon Press. 598.
14. R.J. Carlton, J.T. Hunter, D.S. Miller, R. Abbasi, P.C. Mushenheim, L.N. Tan, and N.L. Abbott, *Chemical and biological sensing using liquid crystals*. Liquid crystals reviews, 2013. **1**(1): p. 29-51.